The metabolome alters the thermodynamic and chemical stability of RNA

ABSTRACT: Herein, we examine the complex network of interactions among RNA, the metabolome, and divalent Mg^{2+} in conditions that mimic the *E. coli* cytoplasm. We determined Mg^{2+} binding constants for the top 15 *E. coli* metabolites, comprising 80% of the total metabolome, at physiological pH and monovalent ion concentrations. This information was used to inform development of artificial cytoplasms that mimic *in vivo E. coli* conditions, termed "Eco80". We empirically determined that the mixture of *E. coli* metabolites in Eco80 approximates single site binding behavior towards Mg^{2+} in the biologically relevant free Mg^{2+} range of ~0.5 to 3 mM Mg^{2+}, using a Mg^{2+} sensitive fluorescent dye . Effects of Eco80 conditions on the thermodynamic stability, chemical stability, structure, and catalysis of RNA were examined. We find that Eco80 conditions lead to opposing effects on the thermodynamics and chemical stability of RNA. The thermodynamic stability of RNA helices was weakened but chemical stability, compactness, and catalysis of RNA were enhanced, dependent on the speciation of Mg^{2+} between weak and strong Mg^{2+}-metabolite complexes in Eco80. Thus, the effects of Eco80 enhance RNA function and increase the biological relevance of mechanistic studies of RNA *in-vitro*.

Introduction

RNA serves as the conduit of genetic information in the Central Dogma of Molecular biology and performs numerous essential functions in all aspects of cellular biology because of its capacity to form complicated, diverse, and functional structures.[1] The development of genome wide structure-probing techniques *in vivo* has provided valuable insight into RNA structure and function cells.[2–4] However, most experimental techniques that provide valuable insight into the mechanism and function of RNA cannot be performed in a cell, and are limited to simple conditions, usually 100 to 500 mM monovalent metal ions and 0.5 to 50 mM free divalent magnesium ions (Mg^{2+}) with a dilute buffer.[5] I*n vitro* studies of RNA in conditions that mimic a cell, so called *in vivo*-like conditions, provide a valuable link between experiments that probe RNA structure *in vivo* and experiments that provide mechanistic and thermodynamic insight *in vitro*.[5]

Many studies have investigated the effects of individual components of the cellular environment on nucleic acid structure, including small molecule and a-biological crowders. Studies that use small molecules and ions that are similar to metabolites in cells indicate that small molecules and ions that interact strongly with the unfolded state of nucleic acids destabilize RNA and DNA secondary structure.[1–5] Studies that simulate the crowding effects of macromolecules found in cells indicate that crowding effects in cells stabilize RNA tertiary structures, increase folding cooperativity, and improve RNA function.[6–10] Thermodynamic characterization of RNA helix formation in crowding conditions indicates crowders destabilize helices and that the nearest neighbor model for calculating RNA structure applies in conditions that mimic the cell.[11–13] In summary, using simple models to simulate elements of the cellular environment *in vitro* has provided valuable mechanistic insight into how the cell effects nucleic acid structure and motivate investigation of more complicated and realistic artificial cytoplasms.[14]

A number of studies have performed mechanistic studies of proteins in extremely complicated environments,[15] ranging from to cell lysates to live cells.[16–18] Such top down approaches to complexity provide valuable insight into how proteins behave in the cell. However, researchers sacrifice the control over the environment that is provided by a simple systems. Mechanistic studies of RNA in the cell or lysate have two additional problems. The first is the propensity of cells to degrade foreign RNA.[19,20] The second is the lack of control of Mg^{2+} speciation between free and chelated Mg^{2+} in lysate because a cell will cease to regulate Mg^{2+} concentrations once it is lysed.

Control over Mg^{2+} speciation is crucial for mechanistic studies of RNA because of the sensitivity of RNA folding and function to the concentration of Mg^{2+} in the solution, as thousands of studies have demonstrated.[21] Recent studies have demonstrated the importance of weak metabolite-Mg^{2+} complexes to RNA function.[22–24] These studies consider effects of 1-3 metabolites at a time which is far from the true complexity of the cellular environment. In addition, Mg^{2+} speciation is approximate in these studies, as Mg^{2+} speciation is estimated assuming single-site-binding, meaning that one metabolite interacts with one Mg^{2+}, and binding constants are extrapolated from published sources, which use different ionic compositions and pHs.[21]

Herein, we take a bottom up, *aufbau*, approach that builds up complexity, to make an artificial cytoplasm that contains 80% of *E. coli* metabolites with biologically relevant concentrations of monovalent ions and free Mg^{2+} ions. We start by compiling metabolite concentrations in *E.* coli, simplify to the 15 most abundant metabolites, determine metabolite-Mg^{2+} binding constants at the relevant pH and ionic strength, and lastly determine how Mg^{2+} in the final mixture of metabolites. This *aufbau* approach allows us to

understand the effects of 80% of metabolite and metal ion species that compose a part of the network of interactions that RNA experiences in *E. coli* cells.

Results

Eco80: An artificial cytoplasm containing 80% of *E. coli* metabolites

E. coli cells contain hundreds of metabolites (~240 mM total), which is too many metabolites to test systematically.[25] However, the 15 most abundant metabolites in *E. coli*, an experimentally manageable number, comprise 80% (195 mM) of total metabolites (Figure 1A). Thus, we sought to prepare Eco80, an artificial cytoplasm containing the biological concentrations of the 15 most abundant metabolites in *E. coli* (Table 1).

Eco80 was prepared at a 2x final concentration so that it could be diluted into other reagents for experiments and contain physiological concentrations of monovalent metal ions at pH 7.0 (see supplementary information (SI) table 1 for details). Briefly, all metabolites in Eco80 are zwitterions or negatively charged near physiological pH 7, which requires electrostatic neutralization with metal ions. Metabolite salts and free acids were prepared to a final 2xconcentration, and the amount of Na^+ and K^+ added with each metabolite was recorded. Next, the pH of the 2xstock was adjusted to pH 7.0 using NaOH, and the amount of Na^+ was recorded. Lastly, NaCl and KCl were added to a final 480 mM Na^+ and 280 mM K^+, twice the physiological value of 240 mM Na^+ and 140 mM K^+. The 2x concentrated artificial cytoplasm was then diluted into other reagents to a final 1x concentration for experiments.

Next, we considered how metabolites affect the speciation of free and chelated Mg^{2+}. All 15 Eco80 metabolites have functional groups, carboxylates and phosphates, that drive chelating interactions with Mg^{2+} ions (Table 1), and we have previously estimated that the metabolite pool in *E. coli* has potential to chelate 51 mM Mg^{2+}, assuming 2 mM free Mg^{2+}, at an ionic strength of 0.15 M and a pH of 7.5.[21] While extensive literature exists on chelating interactions between Mg^{2+} and small molecules, our previous estimates are approximate as Mg^{2+} binding affinity is dependent on environmental factors such as pH, ionic strength, composition of background ions, and temperature.[26–32] Thus, we sought to better characterize Mg^{2+} chelation by the metabolites in Eco80, at the physiological background.

We determined apparent disassociation constants (K_D) for Eco80 metabolites in 240 mM NaCl, 140 mM KCl, pH 7.0 buffer at 37 °C (Table 1). Isothermal titration calorimetry (ITC) was used to measure K_Ds for phosphorylated metabolites (SI figure 1, SI Table 2). A fluorescence assay, that measures the free Mg^{2+} concentration in a sample using the metal ion binding dye 8-Hydroxy-5-quinolinesulfonic (HQS) acid,[33] was used to estimate the K_D for Mg^{2+} of metabolites that did not produce enough heat on binding Mg^{2+} to measure with ITC (SI figure 2, SI Table 3). For the HQS assay, Mg^{2+} is titrated into HQS solutions in the absence and presence of chelators. HQS emission as a function of the total Mg^{2+} in the absence of chelators is then fit to a binding model (SI figure 2A, top blue data and black fit). The free Mg^{2+} concentration is then calculated from the fluorescence emission for each data point using the binding model, providing the free Mg^{2+} concentration as a function of the total Mg^{2+} concentration (SI figure 2A, bottom). Mg^{2+} binding by metabolites is thus obtained by fitting the free Mg^{2+} concentration as a function of the total Mg^{2+} concentration, which is shifted to the right as Mg^{2+} is sequestered by metabolites.

The binding affinity for Eco80 metabolites and Mg^{2+} range from extremely strong to negligible. The four nucleotide triphosphates, ATP, UTP, GTP, and dTTP, were classified as strong Mg^{2+} binders, with K_D values less than the approximate free Mg^{2+} concentration in *E. coli* of 2 mM (Table 1). Conversely, 8 other metabolites, L-glutamic acid, fructose 1,6-BP, UDP-N-acetylglucosamine, glucose 6-phosphate, L-aspartic acid, 6-phospho-gluconic acid, dihydroxyacetone phosphate, and pyruvic acid were classified as weak Mg^{2+} binders, with a K_D value greater than 2 mM (Table 1). Three metabolites, glutathione, L-valine, and L-glutamine had negligible Mg^{2+} binding properties, as measured with HQS (SI figure 2). In an effort to understand the effects of Eco80 on RNA mechanistically, we created two sub-artificial cytoplasm: NTP chelated Mg^{2+} (NTPCM), and weak metabolite chelated Mg^{2+} (WMCM), composed of the strong Mg^{2+} chelators (NTPs), and weak Mg^{2+} chelators, respectively (Table 1).

We used two methods to estimate how Eco80 metabolites affect the speciation of free and chelated Mg^{2+} as a mixture. The first method was the same HQS assay that we used to estimate binding constants for metabolites that did not produce enough heat on Mg^{2+} binding to measure with ITC, based on calculating the free Mg^{2+} concentration in the presence of metabolites using HQS fluorescence emission (Figure 1B-C, SI Table 4). The second method to determine Mg^{2+} speciation was a statistical model that

accounts for experimental uncertainty in metabolite concentrations and uncertainty in K_D determination, and estimates Mg^{2+} speciation assuming single-site binding (meaning that one metabolite associates one Mg^{2+}). This model is described in detail in the Supplementary Methods. Briefly, concentration errors were propagated from uncertainties in reagent masses and volumes used during sample preparation, and K_D uncertainties were obtained from the fits (Table 1). Both uncertainties were then randomly seeded into Equation 1 to create 1000 virtual artificial cytoplasms, where $[Mg]_T$ is the total Mg^{2+} concentration, [Mg] is the free Mg^{2+} concentration, "*i*" is an integer representing each metabolite in a mixture, N is the total number of metabolites in a mixture, $[L_i]_T$ is the concentration of the "*i'th*" metabolite in a mixture, and K_D is the disassociation constant.

$$[Mg]_T = [Mg] + \sum_{i=1}^{N} \frac{[L_i]_T [Mg]}{K'_{D\,i} + [Mg]} \quad (1)$$

Then, equation 1 is solved numerically to determine the free Mg^{2+} concentration produced at a given total Mg^{2+} concentration in a virtual artificial cytoplasm.

The two methods indicate that Mg^{2+} speciates in artificial cytoplasms according to a single-site model within or below the biological free Mg^{2+} range of 0.5 to 3 mM Mg^{2+}. However, Mg^{2+} does not speciate according to a single-site model at higher free Mg^{2+} concentrations (Figure 1 E-F). In Eco80, the statistical model suggests that the metabolites should buffer the free Mg^{2+} concentration in the biological Mg^{2+} range, where a 20 mM increase in the total Mg^{2+} from 20 to 40 mM leads to a 2.5 mM increase in free Mg^{2+} from 0.5 to 3 mM (Figure 1E, hex bins). Free Mg^{2+} concentrations measured in this range with HQS emission are consistent with this single-site behavior (Figure 1E, data points). At higher free Mg^{2+} concentrations, Eco80 should lose its free Mg^{2+} buffering capacity as chelators become saturated, and the free Mg^{2+} should increase with the total Mg^{2+} (Figure 1E, hex bins). However, the free Mg^{2+} concentration measured with HQS does not increase as fast as the statistical model predicts above 3 mM free Mg^{2+} (Figure 1E, data points). For example, free Mg^{2+} in Eco80 is expected to increase from 3 mM to ~100 mM as the total Mg^{2+} concentration is increased from 40 mM to 200 mM (Figure 1E, hex bins). However, the free Mg^{2+} concentration measured with HQS only increases from 3 mM to ~10 mM (Figure 1E, data points). One possibility is that multivalent interactions, which the statistical model does not account for, where several Mg^{2+}-saturated metabolites interact with additional Mg^{2+} molecules, dominate the equilibrium. Such non-single-site behavior above 3 mM free Mg^{2+} is also observed in the NTPCM and WMCM artificial cytoplasms (Figure 1 F & G), and was observed previously.[21]

Lastly, we sought to empirically determine how much total Mg^{2+} is required to attain a free Mg^{2+} concentration of 2 mM in Eco80, NTPCM, and WMCM. The relationship between the free Mg^{2+} calculated from HQS emission and the total Mg^{2+} concentration in each artificial cytoplasms was fit to a polynomial to empirically approximate the data (Figure 1 E-G, blank lines), and the total Mg^{2+} concentration required to produce 2 mM Free Mg^{2+} was calculated from the polynomial fit (see methods for details). This resulted in predicted 31.6, 25.0, and 6.5 mM total Mg^{2+} concentration to produce 2 mM free Mg^{2+} in Eco80, NTPCM, and WMCM, respectively (Table 2).

Thermodynamic analysis of RNA helices in Eco80

We sought to understand how Eco80 affects the thermodynamic stability of RNA. We began on RNA helices composed of Watson-Crick base pairs. RNA helix stability is traditionally measured with UV-absorbance melting curves, typically monitored at 260 or 280 nm. [34,35] However, such absorbance melting curves were not appropriate for measuring helix stability in Eco80 because of the high absorptivity of ATP, UTP, GTP, dTTP, and UDP-N-acetylglucosamine, which are major components of Eco80. Thus, we designed a fluorescence binding isotherm assay, which is optically orthogonal to Eco80.

Helix stability was measured using the emission of a 5'-fluorophore labeled RNA strand (FAM-RNA) in equilibrium with a complementary 3'-quencher labeled RNA strand (RNA-BHQ1), (Figure 2A). High emission indicates that the FAM-RNA is single-stranded, while low emission indicates that the FAM-RNA is bound in duplex with an RNA-BHQ1 strand. We used a binding isotherm method, where RNA-BHQ1 is titrated into a constant concentration of FAM-RNA at a single temperature (SI figure 3), resulting in an apparent binding isotherm (Figure 2B). Fluorescence binding isotherms were favored over fluorescence melts because of the

unpredictable dependence of FAM emission on temperature.[36–38] Emission of FAM was monitored in a Real-Time PCR instrument at different temperatures, resulting in a isotherm every 0.5 °C from 20 to 80 °C (Figure 2B).

Raw fluorescence was fit with a new program called MeltR, created by the authors, to determine folding energies. MeltR is a package of functions in the popular R programming language, that allows facile conversion of raw data to folding energies (see methods for details). Importantly, MeltR handles two sources of experimental error, uncertainty in RNA concentration and inaccurate K_Ds collected at low and high temperatures. MeltR handles uncertainties in RNA concentration by using a Job plot obtained from fluorescence isotherms at low temperatures. Likewise, MeltR allows the user to select isotherms that provide the most accurate K_Ds, which are then passed to the non-linear regression algorithms that determine helix folding energies. MeltR then calculates folding energies using two Van't Hoff methods, directly fitting a Van't Hoff plot (Figure 3C) and globally fitting raw fluorescence emission to SI equation X. Errors in the main text are reported 1.5% in terms of the $\Delta G^{37^\circ C}$ and a detailed error analysis is in the methods.

Eco80 destabilizes RNA helices

We used fluorescence binding isotherms to determine helix folding energies in background monovalent metal ion control (240 mM NaCl 140 mM KCl), Eco80, NTPCM, and WMCM, for a data set of five representative eight base-pair RNA helices. All solutions contain 2 mM Mg^{2+}, as per Table 2. The helix set contains representatives of all 10 Watson-Crick nearest neighbor parameters, vary in AU content from 25% to 75%, and thus represent a good range of helical features. We used both methods to determine folding energies in MeltR, where method 1 was fitting the Van't Hoff relationship between the disassociation constant and temperature and method 2 was directly globally fitting the raw fluorescence binding isotherms (SI table 5). Results are summarized in Table 3.

All five representative helices were significantly destabilized in Eco80, meaning the $\Delta\Delta G^{37^\circ C}$ between the background monovalent condition and Eco80 was larger than the propagated uncertainty in $\Delta\Delta G^{37^\circ C}$ (Table 3, Figure 2D). We did not observe a clear relationship between AU content and destabilization. For example, Helix 2 has a relatively low AU content of 38% and was strongly destabilized by 1.12 kcal/mol in Eco80. However, helix 1 and 5, the sequences with the lowest (25%) and highest (75%) AU content respectively, were destabilized by the same amount, 0.60 and 0.61 kcal/mol, respectively. Likewise, helices 3 and 4 both have an AU content of 63%, but they were destabilized by different amounts, 0.44 and 0.64 kcal/mol respectively. Thus, Eco80 destabilizes RNA helices but the underlying sequence dependence is currently unclear.

To better understand how components of Eco80 destabilize RNA helices, we then analyzed the effects of strong Mg^{2+} chelating metabolites and weak Mg^{2+} chelating metabolites, separately. NTPCM, which is composed of strong Mg^{2+} chelating metabolites, consistently destabilized RNA helices (Figure 2D). Helices 2, 3, 4, and 5 were significantly destabilized by 0.41 to 0.60 kcal/mol (Table 3). NTPCM did not significantly destabilize Helix 1, however, the 0.32 kcal/mol destabilization effect is consistent with the other 5 helices. In fact, as the AU content of helices increases the destabilization increases steadily from 0.32 kcal/mol at a 25% to 0.60 kcal/mol at 75% with a slope of 5.5 cal/mol/percent AU content (R^2 = 0.99, SI figure 4).

In contrast to NTPCM, WMCM, which is composed of weak Mg^{2+} chelating metabolites, destabilized, had no effect, or stabilized RNA helices depending on the helix identity (Figure 2D). Similar to Eco80, the sequence dependence of stabilization or destabilization is not clear. No significant change in stability was observed for helices 3 and 4 in WMCM and both have an AU content of 63%. Helix 1 and 5, with the lowest and highest AU content of 25% and 75% respectively, were destabilized by 0.40 and 0.82 kcal/mol in WMCM. In contrast, Helix 2, with an intermediate AU content of 38% was stabilized in WMCM.

Thus, the net effect of Eco80 on RNA helices is destabilization, with destabilizing interactions dominating for strong Mg^{2+} chelating metabolites, and a mixture of stabilizing and destabilizing interactions for weak Mg^{2+} chelating metabolites.

Eco80 protects RNA from degradation

Several studies indicate that weak and strong Mg^{2+} chelating metabolites reduce Mg^{2+} mediated RNA degradation and we hypothesized that Eco80 could also protect RNA from degradation.[22,39] We used an in-line degradation (in-line probing) assay to determine if Eco80 stabilizes the chemical structure of RNA. In-line probing takes advantage of the natural susceptibility of the RNA phosphodiester backbone to cleavage.[40] In this mechanism, the 2'-hydroxyl is deprotonated by a hydroxide anion (often facilitated by an Mg^{2+}), and the 2'-hydroxyl serves as a nucleophile to replace the 5'-hydroxyl of the next nucleotide, in an SN2-like mechanism (Figure 3A). Unstructured nucleotides are more susceptible to cleavage because they are more likely to adopt an in-line

conformation that favors cleavage. For this assay, 5'-P^{32} RNA are incubated at 37 °C for about 90 hours to facilitate in-line cleavage. RNA fragments are then fractional on a denaturing PAGE gel, providing single nucleotide resolution of cleavage rates, measured by the increase in counts with time for a given band (SI figure 5).

We first determined in-line degradation rates for the guanine riboswitch aptamer (Figure 3B). The guanine riboswitch aptamer is a highly structured RNA aptamer that binds the guanine nucleobase, and has been studied extensively, thus providing structural and mechanistic information.[1–3] Moreover, the apo (guanine ligand un-bound) state and the guanine ligand bound state are similar, showing structural changes only in the nucleotides that directly mediate the guanine binding site.[1]

Degradation rates for nucleotides 29 to 63 in Eco80, NTPCM, and WMCM with enough total Mg^{2+} to maintain 2 mM free Mg^{2+} were compared to degradation rates in a 2 mM free Mg^{2+} and 25 mM free Mg^{2+}. The 25 mM free Mg^{2+} condition was chosen because it is a common free Mg^{2+} condition *in-vivo* and is similar to the 25 and 31.6 total Mg^{2+} condition used for NTPCM and Eco80, respectively (Table 2). Degradation fragments greater than 63 could not be resolved on the gel and degradation fragments shorter than 29 were smeared out because of the high concentrations of negatively charged ions in the samples (SI figure 5). Overall, the guanine riboswitch aptamer exhibited similar degradation patterns between the 2 mM free, Eco80, NTPCM, and WMCM conditions, with high degradation in the 5'-region of the P2 stem and high reactivity in the P3-stem loop region (Figure 3C). This indicates that the guanine riboswitch aptamer adopts a similar structure in these conditions (SI figure 6). The 25 mM free condition, exhibited higher degradation rates in the P2-P3 junction (Figure 3C). This pattern is similar to ILP data published for another guanine riboswitch aptamer, but in a high Mg^{2+} condition and pH 8.0, indicating that the increase in degradation rates in the 25 mM free Mg^{2+} condition is dependent on the presence of Mg^{2+}-OH^- complexes (SI figure 6).

To confirm that the guanine aptamer adopts similar structures between all conditions, we collected small angle X-ray scattering (SAXS) data in every artificial cytoplasm. Raw scattering overlay, indicating that the structure of the guanine aptamer is similar between conditions (SI figure 7A). Guinier analysis and p(r) analysis, where the maximum is the radius of gyration (SI figure 7B), indicate that the radius of gyration is similar between solution conditions (SI table 6). Lastly, electron density reconstructions and bead model reconstructions are consistent with the known structure of the guanine riboswitch aptamer in every condition (Figure 3D, SI Figure 7C-G). Thus, decreased degradation rates in the 2 mM free, Eco80, NTPCM, and WMCM conditions in comparison to the 25 mM free condition is likely due to a reduction in the availability Mg^{2+}-OH^- complexes caused by chelation of Mg^{2+} by metabolites rather than changes in RNA structure.

We sought to better characterize the structural dependence of guanine aptamer degradation in different conditions. We examined the crystal structure for the guanine riboswitch aptamer and classified each residue as single stranded, meaning that the base was not participating in hydrogen bonding interactions with other residues, non-canonical, meaning that the base was forming non-canonical hydrogen bonding interactions with other residues, Watson-Crick (WC), meaning that the base was in a traditional Watson-Crick base pair with another residues, Watson-Crick + Non-canonical (WC + NC), meaning that the base was forming a traditional Watson-Crick base pair with another residues and participating in a non-canonical contact.

We observed decreased degradation rates at the single stranded nucleotide U39 in 2 mM free Mg^{2+}, Eco80, NTPCM, and WMCM, in comparison to the 25 mM free Mg^{2+} condition. Likewise, we observed an overall decrease in reactivity in 2 mM free Mg^{2+}, Eco80, NTPCM, and WMCM in comparison to the 25 mM free Mg^{2+} condition for nucleotides involved in non-canonical tertiary interactions. In contrast, degradation rates for nucleotides participating in Watson-Crick base pairing interactions were independent across solution conditions. Interestingly, the overall decrease in degradation rates in artificial cytoplasm, in comparison to the 25 mM free Mg^{2+} condition, was observed for nucleotides that participate in Watson-Crick base pairs and participate in a second hydrogen bonding interaction with the base of another residue. Thus, we observed a trend of protection from Mg^{2+} mediated degradation in artificial cytoplasm composed of Mg^{2+} chelating metabolites in comparison to the 25 mM free Mg^{2+} condition, even with similar amounts of total Mg^{2+} in solution.

We repeated our in-line degradation assay with two other highly studied biological RNA, the cleaved- CPEB3 ribozyme and yeast $tRNA^{phe}$, to confirm that a reduction of Mg^{2+} mediated degradation in artificial cytoplasm was a broadly applicable trend (SI figure 8, 9, & 10). For the cleaved-CPEB3 ribozyme, degradation rates at singles stranded residues were reduced in Eco80 and WMCM in comparison to the 25 mM free Mg^{2+} condition (Figure 3F). The degradation rates for a residue that is predicted to participate in a

non-canonical tertiary contact was reduced in Eco80 but not WMCM, in comparison to the 25 mM free Mg^{2+} condition. Degradation rates were constant for nucleotides participating in Watson-Crick base-pairs for the cleaved-CPEB3 ribozyme, between the 2 mM free Mg, the Eco80, and the 25 mM condition Mg conditions, like the guanine riboswitch aptamer. Interestingly, Degradation rates in the NTPCM condition were reduced for all structure classifications compared to all other conditions. Yeast $tRNA^{phe}$ exhibits almost no in-line degradation except for the single stranded nucleotides in the P3 stem loop, termed the anticodon loop (SI figure 9D), consistent with published data. Single stranded nucleotides, mostly from the anticodon loop showed reduced degradation rates in the in Eco80, NTPCM and WMC in comparison to the 25 mM free condition, like the guanine riboswitch aptamer and the CPEB3 ribozyme. Likewise, degradation rates were constant across conditions for nucleotides that form Watson-Crick base pairs, similar to the guanine riboswitch aptamer and the CPEB3 ribozyme. However, degradation rates were constant across conditions for nucleotides that form non-canonical contacts, which is different than the increased degradation observed for nucleotides that form non-canonical base pairs in the guanine riboswitch aptamer and the CPEB3 ribozyme. One possible explanation is that the tertiary structure of $tRNA^{phe}$ is less dynamic than the tertiary structure of the guanine riboswitch aptamer and the CPEB3 ribozyme.

Thus, overall, the in-line degradation assay indicated that Eco80, NTPCM, and WMCM protect RNA from Mg^{2+} mediated degradation, even though all three artificial cytoplasm's have relatively high concentrations of Mg^{2+}. This protective effect is enhanced in unstructured regions where RNA is most susceptible to Mg^{2+} mediated degradation.

The weak Mg^{2+} chelating metabolites in Eco80 promote RNA catalysis

Weak metabolite chelated Mg^{2+} is known to promote catalysis by ribozymes. For example, the CPEB3 ribozyme catalysis is enhanced by about 1.6-fold by 2 mM free Mg^{2+} in solution with an estimated 11.3 mM free glutamate chelated Mg2+, in comparison to catalysis in 2 mM free Mg^{2+} alone. Thus we also hypothesized that Eco80 metabolites would also promote CPEB3 catalysis.

We measured CPEB3 ribozyme cleavage rates in 2 mM free Mg^{2+}, a total 25 mM free Mg^{2+}, and Eco80, NTPCM, and WMCM containing enough total Mg2+ to produce 2 mM free Mg^{2+} (Table 2). Briefly, we purified full length CPEB3 ribozyme (Figure 4A), incubated CPEB3 in artificial cytoplasm's, fractionated cleaved and un-cleaved CPEB3 from time points on a denaturing acrylamide gel, and calculated the fraction cleaved from the relative intensity of cleaved and un-cleaved RNA bands (SI Figure 10). Fraction cleaved as a function of time was fit to a single exponential equation to estimate the reaction rate (Figure 4B). We performed 4 reactions per condition.

CPEB3 ribozyme catalysis was reduced in all conditions in comparison to the 25 mM free Mg^{2+} control (Figure 4C). Surprisingly, CPEB3 catalysis was one half as fast in Eco80 in comparison to the 2 mM free Mg^{2+} control, despite the 31.6 mM total Mg^{2+} in Eco80. Likewise, CPEB3 catalysis was one third as fast in NTPCM in comparison to the 2 mM free Mg^{2+} control, an even stronger effect than Eco80. In contrast, CPEB3 catalysis was enhanced by 1.33 fold in WMCM, similar to the enhancement observed for glutamate chelated Mg^{2+}.In summary, the artificial cytoplasm composed of weak Mg^{2+} chelating metabolites with 2 mM free Mg^{2+} enhanced CPEB3 catalysis, the artificial cytoplasm composed of strong Mg^{2+} chelating metabolites 2 mM free Mg^{2+} reduced CPEB3 catalysis, and the mixture of both types of metabolites had an intermediate effect.

Discussion

Making Eco80 artificial cytoplasm

-Complex but manageable

Free Mg^{2+} buffering in the cell

-Has been observed by Email Phil for Papers

Effects on helices

-Mg stabilizes (from lit)

-Polor osmolytes destabilize (from lit)

-Allison's paper

This type of sequence dependence of destabilization by nucleotides has been observed for G-quadruplex RNA, but in reverse, where the identity of the nucleotide in the solution matters. In this case, cytidine nucleotides destabilized G-quadruplex structure, but the other nucleotides did not.

-Here we analyze their effects together and see opposing effects

Propose model that summaries effects

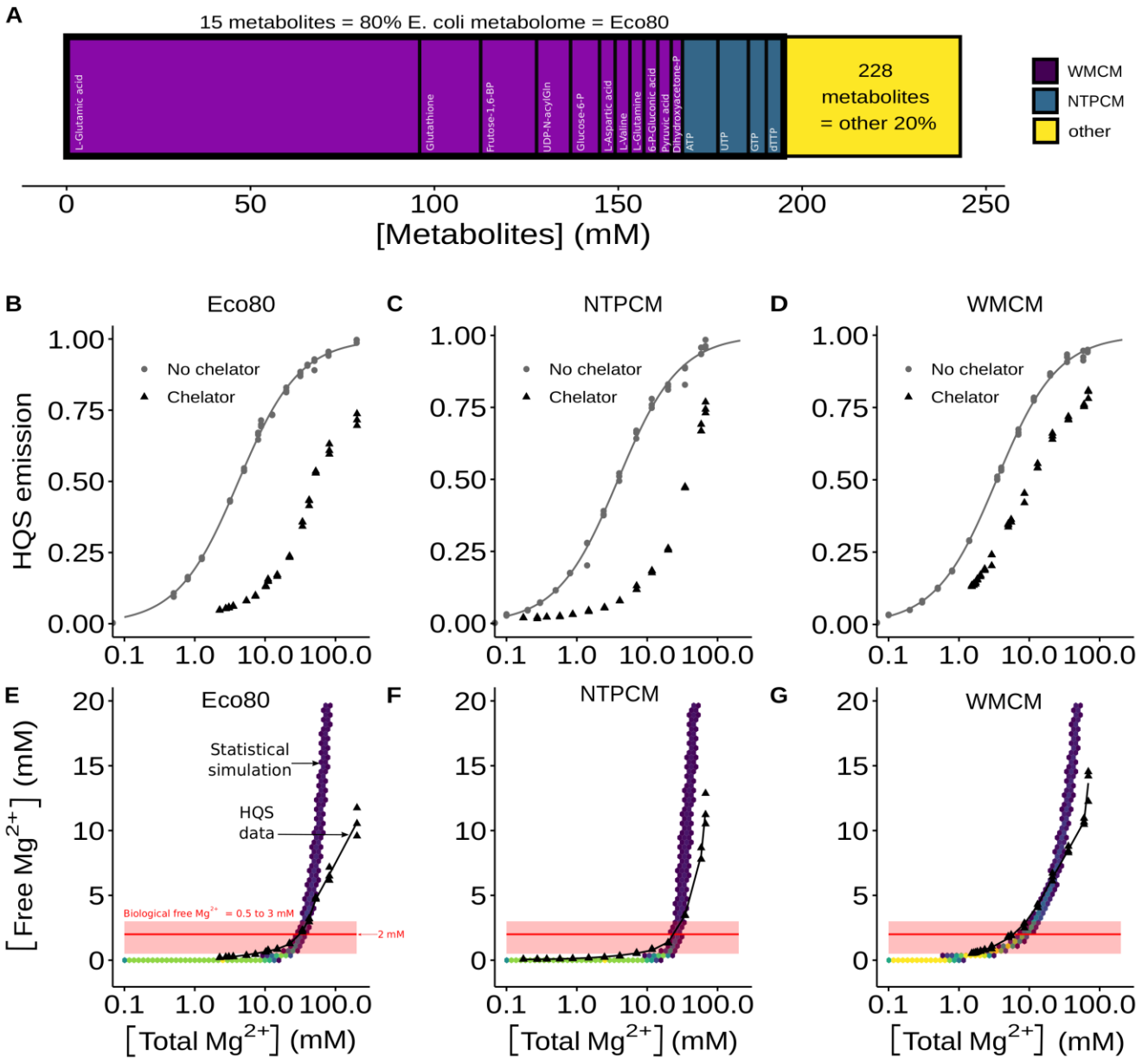

Figure 1 Analysis of Mg^{2+} speciation in *E. coli* metabolite mixtures. **(A)** E. coli metabolome molar composition. Eco80 contains the 15 most abundant metabolites that comprise 80% of the *E. coli* metabolome. NTPCM contains four strong Mg^{2+} chelating NTPs, and WMCM contains 11 other weak Mg^{2+} binding metabolites. **(B-D)** Effect of Mg^{2+} on 8-hydroxyquinoline-5-sulphonic acid (HQS) emission with and without mixtures of metabolites that chelate Mg^{2+}. Grey lines represent fits to determine the binding constant for Mg^{2+} and HQS in the absence of chelators. **(E-G)** Relationship between the total Mg^{2+} concentration and the free Mg^{2+} concentration with mixtures of metabolites that chelate Mg^{2+}. The free Mg^{2+} concentration (y-axis) was calculated using HQS emission and the binding constant for Mg^{2+} and HQS. Hex bins represent 1000 statistical simulations of the virtual artificial cytoplasms based on experimental errors in K_D determination, experimental errors in reagent concentrations, and single site binding. Triangle data points are free Mg^{2+} concentrations calculated using HQS emission. Black lines were generated using polynomial regression. The red shaded region is the biological free Mg^{2+} concentration, 0.5 to 3 mM. The red line is the approximate free Mg^{2+} concentration in *E. coli* of 2 mM.

Table 1. Eco80: the 15 most abundant metabolites which comprise 80% of the *E. coli* metabolome.

Metabolite	Conc. (mM)[a]	K_D (mM)	Chelation strength[e]
ATP	9.63 (0.963)	0.28 (0.01)b	NTPCM (Strong)
UTP	8.29 (0.829)	0.248 (0.004)[b]	NTPCM (Strong)
GTP	4.87 (0.487)	0.201 (0.007)[b]	NTPCM (Strong)
dTTP	4.62 (0.462)	0.160 (0.003)[b]	NTPCM (Strong)
L-Glutamic acid	96 (9.6)	520 (50)[c]	WMCM (Weak)
Glutathione	16.6 (1.66)	NA[d]	WMCM (Weak)
Fructose 1,6-bisphosphate	15.2 (1.52)	5.9 (0.1)[b]	WMCM (Weak)
UDP-N-acytylglucosamine	9.24 (0.924)	29 (2)[b]	WMCM (Weak)
Glucose 6-phosphate	7.88 (0.788)	17.3 (0.2)[b]	WMCM (Weak)
L-Aspartic acid	4.23 (0.423)	465 (12)[c]	WMCM (Weak)
L-Valine	4.02 (0.402)	NA[d]	WMCM (Weak)
L-Glutamine	3.81 (0.381)	NA[d]	WMCM (Weak)
6-Phospho-gluconic acid	3.77 (0.377)	14.4 (0.2)[b]	WMCM (Weak)
Pyruvic acid	3.66 (0.366)	15.8 (0.9)[c]	WMCM (Weak)
Dihydroxyacetone phosphate	3.06 (0.306)	20 (1)[b]	WMCM (Weak[e])

[a]uncertainty propagated from uncertainties in reagent masses and volumes used during sample preparation. Extra significant digits included to avoid systematic rounding errors in the statistical model.

[b]Determined at 37 °C with Isothermal titration calorimetry as measured in SI figure 1 and SI table 2. Error is the propagated standard error in the fit parameters.

[c]Determined at 37 °C with HQS emission as measured in the SI figure 2 and SI table 3. Error is the propagated standard error in the fit parameters.

[d]No binding observed as per SI Figure 2.

[e]Metabolites with K_Ds for Mg^{2+} less than 2 mM are considered strong Mg^{2+} chelators while metabolites with K_Ds for Mg^{2+} more than 2 mM are considered weak Mg^{2+} chelators.

Table 2. Total Mg^{2+} concentrations used to obtain 2 mM free Mg^{2+} in artificial cytoplasm.

Condition	[Total Mg^{2+}] (mM)	[Chelated Mg^{2+}] (mM)	[Free Mg^{2+}] (mM)
Eco80	31.6	29.6	2.0
NTPCM	25.0	23	2.0
WMCM	6.4	4.5	2.0

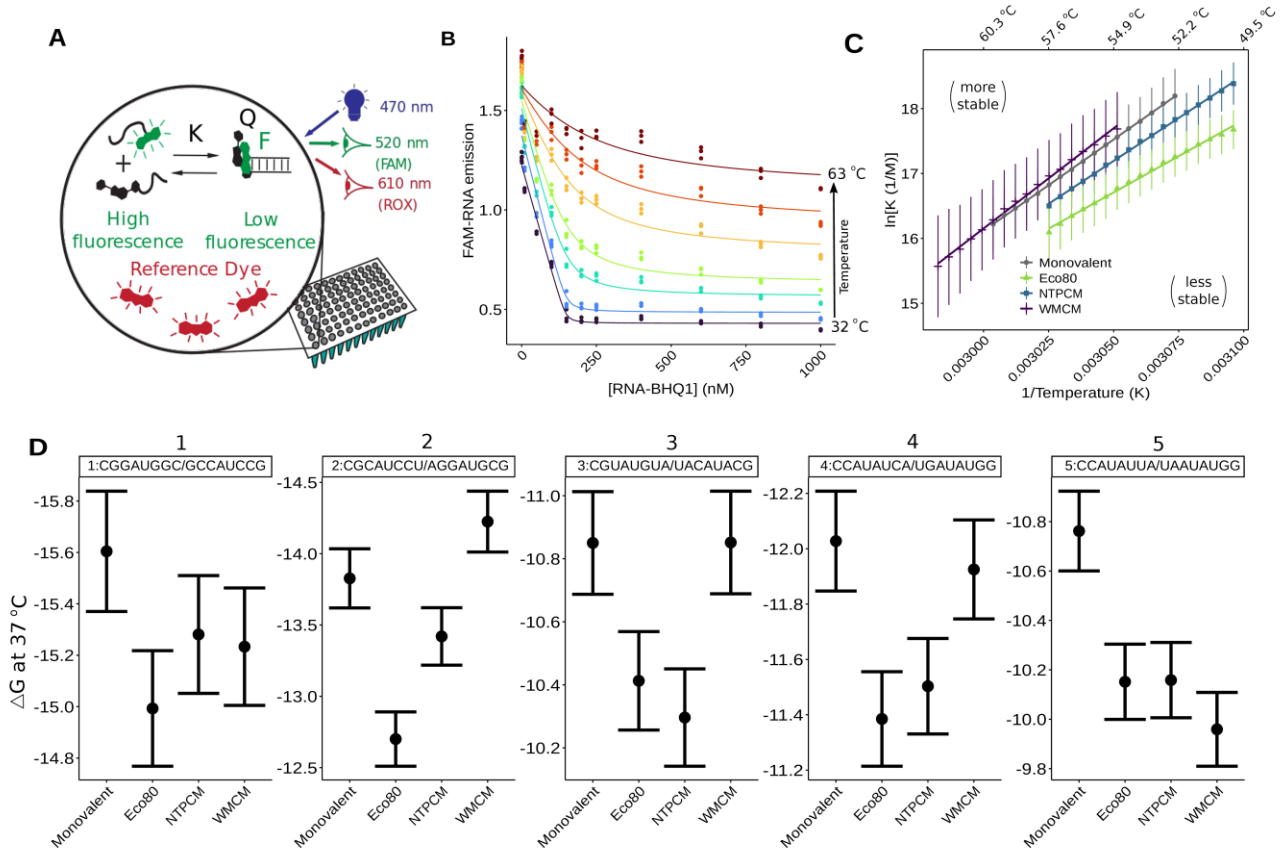

Figure 2 *E. coli* metabolite Mg^{2+} mixtures destabilize RNA secondary structure. Helix folding energies in Eco80, NTPCM, and WMCM were determined using fluorescence binding isotherms that are fit with the MeltR program. **(A)** Layout of a fluorescence binding isotherm assay in a Real-Time PCR machine. **(B)** Raw fluorescence binding isotherms fit to determine equilibrium constants with MeltR. Data points represent raw data. Curves represent curve fits. Colors represent different temperatures (purple: 32.3, blue: 41.8, teal: 51.3, green: 54.6, yellow: 58.4, orange: 60.7, red: 63.1 °C). **(C)** Van't Hoff relationship between equilibrium constant and temperature for helix 2:CGCAUCCU/AGGAUGCG folding in background monovalent metal ions (240 mM NaCl 140 mM KCl), Eco80, NTPCM, and WMCM. All conditions contain 2 mM free Mg^{2+}. Points and error bars represent association constants and standard errors propagated from the fit (using MeltR). Lines represent the fits to the Van't Hoff equation that MeltR uses to calculate folding energies. A shift in the Van't Hoff relationship, down and to the right of the plot area, indicates that Eco80 destabilizes the Helix. **(D)** The Gibbs free energy at 37 °C, $\Delta G^{37°C,}$ in Eco80, NTPCM, and WMCM compared to the $\Delta G^{37°C}$ in background monovalent metal ions (240 mM NaCl 140 mM KCl), for five RNA helices. All conditions contain 2 mM free Mg^{2+}. Errors were propagated assuming 1.% uncertainty in the Gibb's free energy at 37 °C (see methods for error analysis).

Table 3. Stability of RNA helices in *E. coli* metabolite mixtures.

Sequence[a]	AU content	Condition[b]	ΔG (kcal/mol)[c]	ΔΔG (kcal/mol)[c]
1: CGGAUGGC/ GCCAUCCG	25%	2 mM free	-15.60 (0.23)	
		Eco80	-15.00 (0.23)	0.60 (0.32)
		NTPCM	-15.28 (0.23)	0.32 (0.33)
		WMCM	-15.20 (0.23)	0.40 (0.33)
2: CGCAUCCU/ AGGAUGCG	38%	2 mM free	-13.82 (0.21)	
		Eco80	-12.70 (0.19)	1.12 (0.28)
		NTPCM	-13.41 (0.20)	0.41 (0.29)
		WMCM	-14.22 (0.21)	-0.40 (0.30)
3: CGUAUGUA/ UACAUACG	63%	2 mM free	-10.85 (0.16)	
		Eco80	-10.41 (0.16)	0.44 (0.23)
		NTPCM	-10.30 (0.15)	0.55 (0.22)
		WMCM	-10.85 (0.16)	0.00 (0.23)
4: CCAUAUCA/ UGAUAUGG	63%	2 mM free	-12.02 (0.18)	
		Eco80	-11.38 (0.17)	0.64 (0.25)
		NTPCM	-11.50 (0.17)	0.52 (0.25)
		WMCM	-11.90 (0.18)	0.12 (0.25)
5:CCAUAUUA/ UAAUAUGG	75%	2 mM free	-10.76 (0.16)	
		Eco80	-10.15 (0.15)	0.61 (0.22)
		NTPCM	-10.16 (0.15)	0.60 (0.22)
		WMCM	-9.94 (0.15)	0.82 (0.22)

[a]The first sequence was 5'-FAM labeled and the second sequence was 3'-BHQ1 labeled.
[b]All solutions contain 2 mM Free3 Mg, 240 Na^+ 140 mM K^+.
[c]Extra significant digits were included to avoid propagating rounding errors.

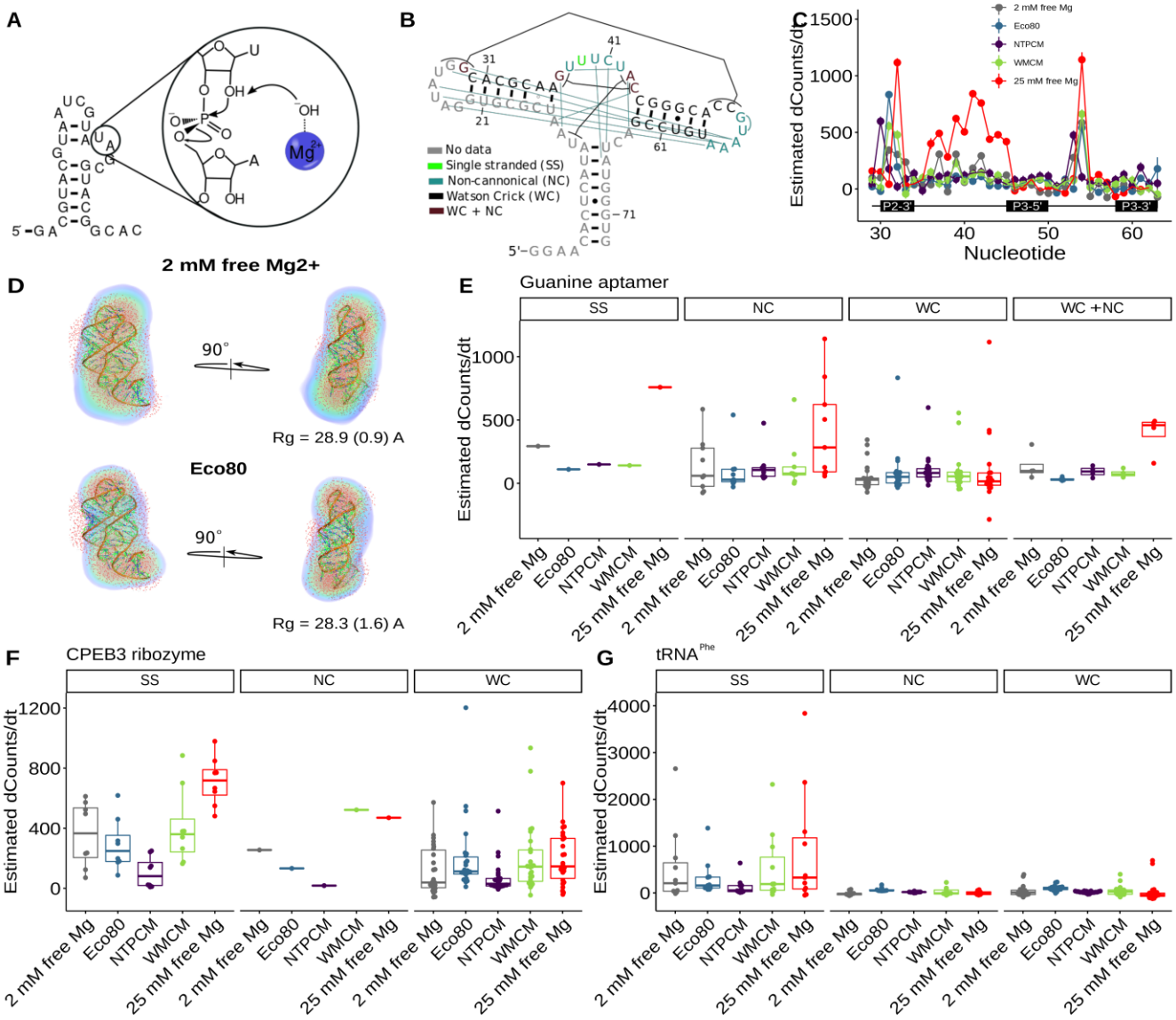

Figure 3 *E. coli* metabolite and Mg^{2+} mixtures stabilize the chemical structure of RNA. **(A)** In-line RNA degradation mechanism facilitated by Mg^{2+}. **(B)** Secondary structure of the guanine riboswitch aptamer with tertiary contacts represented by colored lines. **(C)** Degradation rate, by the increase in counts as a function of time at each residue in different solution conditions as a function of location in the RNA. Points represent the slope for the line of best fit and error bars represent the standard error in the slope estimated from the fit. **(D)** Small angle x-ray scattering (SAXS) analysis of the guanine riboswitch aptamer in artificial cytoplasm indicates that the RNA adopts a similar structure. Electron density maps generated with DENSS are superimposed on the crystal structure of the guanine aptamer (PDB: 1U8D), modified by removing the hypoxanthine ligand and modeling in a solvent shell using WAXSiS. **(E-F)** Estimated increase in counts as a function of time, in different conditions grouped by the structure each nucleotide, based on analysis of crystal structures and covariation models.

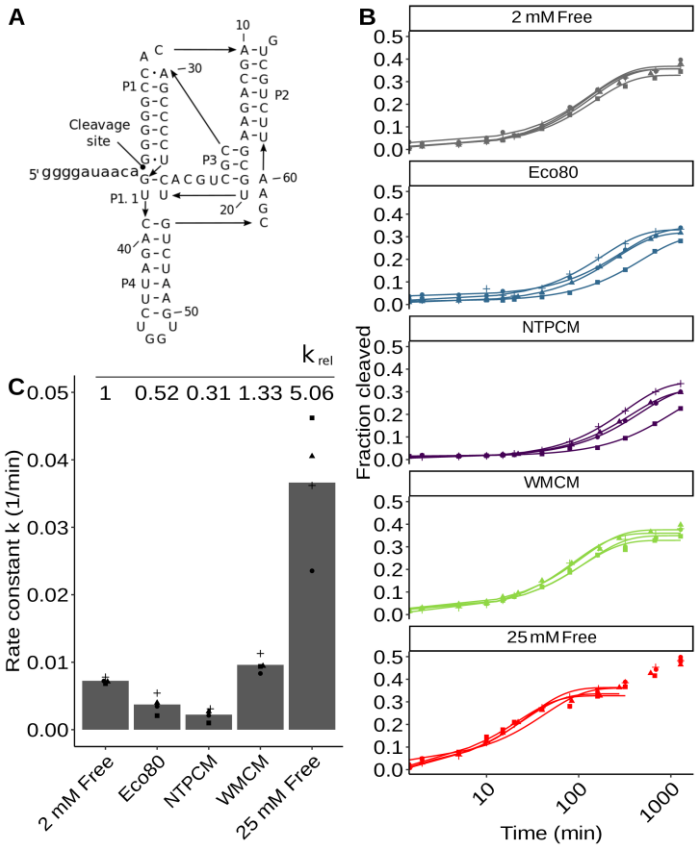

Figure 4 *E. coli* metabolite and Mg^{2+} mixtures stabilize the chemical structure of RNA. **(A)** In-line RNA degradation mechanism facilitated by Mg^{2+}

Automatic citation updates are disabled. To see the bibliography, click Refresh in the Zotero tab.